Acta Avionica Volume XXVI, 52 – No.1, 2025, DOI: 10.35116/aa.2025.0008

EXPERIMENTAL STUDY ON RADIAL COMPRESSOR INSTABILITY CAUSED BY INLET AIRFLOW RESTRICTION

Marián HOCKO, Maroš DIVOK, Maksym PETRENKO
Technical University of Kosice Faculty of Aeronautics, Rampova 1731/7, 040 01 Kosice, Slovakia
**Corresponding author.* E-mail: marian.hocko@tuke.sk

Abstract. This work examines the issue of unstable performance in aircraft turbine engine compressors, focusing on radial compressors. It investigates the causes, mechanisms, and effects of compressor instability, such as airflow pulsations, pressure variations, engine vibrations, and the risk of compressor blade damage. The theoretical section explains how deviations in airflow rate from design specifications can result in flow separation and a transition from laminar to turbulent flow, which may lead to surge and possible reverse airflow.

The analysis of real MPM-20 engine measurements and results for key parameters such as pressures, temperatures, and airflow rates showed significant agreement with models, confirming the theoretical assumptions. These findings underline the crucial role of stable airflow management and effective compressor design in maintaining the safe operation of aircraft engines, especially under varying and extreme flight conditions.

Keywords: engine test, radial compressor instability

1. INTRODUCTION

A key issue in aircraft turbine engines is unstable compressor performance, often caused by non-ideal conditions. Though rare in normal flight, it can threaten engine reliability and safety, characterized by fluctuations in airflow, outlet pressure, and airspeed, potentially leading to surge or flow reversal. This phenomenon is characterized by sudden and repetitive fluctuations in airflow velocity (Qv), outlet pressure (p2), and absolute airspeed (c). In the more severe cases, these disturbances can lead to compressor surge or flow reversal, where the airflow moves backward towards the engine inlet [1],[11].

Symptoms of unstable work often include pressure changes, noises, vibrations, and blade issues. Causes include intake irregularities, faulty controls, foreign objects, rapid maneuvers, and environmental conditions like fires or volcanic ash. Addressing these factors is vital for stable operation across all flight phases [3]. Compressor instability causes ot airflow separation during deviations, leading to fluctuating airflow and pressure [2]. This study analyzes compressor instability during reduced airflow, examining aerodynamic and thermodynamic effects like flow separation and transition to turbulence, using modeling and empirical tests with the MPM-20 engine to understand causes and impacts on performance.

1.1. Unstable operation of radial compressor

Unstable operation in the engine's radial compressor occurs when airflow across impeller and diffuser blades is interrupted, often due to changes in the angle of attack of incoming air. Fluctuations in airflow rate or rotor speed mainly cause these disruptions.

Instability is most likely to occur when the recalculated compressor speed (n_p) exceeds the nominal design speed $n_{p,cal.}$.

$$n_p = n.\sqrt{\frac{288}{T_{1c}}}[\mathrm{min.}^{-1}] \tag{1.2.1}$$

$$n_p = n.\sqrt{\frac{288}{T_1.\left(1+\frac{\kappa-1}{2}.M_1^2\right)}}[\mathrm{min.}^{-1}] \tag{1.2.2}$$

Where: np - Recalculated speed [min.-1], n - Measured speed [min.-1], T1c - Total air temperature at the inlet to the radial compressor [K]; T1 - Static air temperature at the inlet to the radial compressor [K]; M - Mach number of flight [1].

As described in equation (1.2.1), the lower static temperatures and Mach numbers prevalent at high altitudes can cause elevated listed speeds, resulting in an unstable condition for the compressor. Otherwise, we can define three different modes in which our engine can operate:

1. Stable operation is achieved when the airflow through a radial compressor equals the design value, $Q_v = Q_{v,cal}$. In non-ideal conditions, the flow stays smooth through the edge impeller and diffuser channels, avoiding instability, as can be seen in Figures 1 and 2.

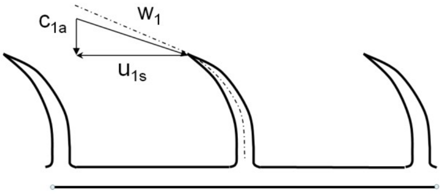

Figure 1 Stable flow around the blades

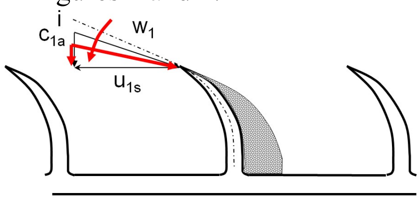

Figure 2 Unstable flow around the blades

2. In cases where airflow exceeds the design rate $Q_v > Q_{v,cal}$, flux separation or entrainment may occur at the impeller blade troughs and behind the vane diffuser blades. This localized swirling flow forms logarithmic spiral-like streamlines, reducing aerodynamic efficiency but usually not causing instability, as seen in Figure 4.

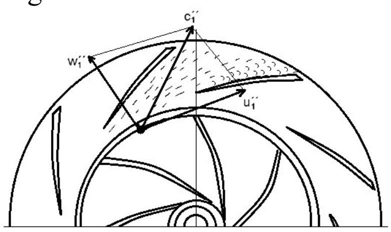

Figure 3 Flow separation on the suction side of the vane diffuser blades, $Q_v > Q_{v,cal}$.

3. When Q_v drops below $Q_{v,cal}$, flow separation occurs behind the impeller blades and in diffuser blade troughs, causing stall (Figure 5). This disrupts flow, reducing velocity and flow area, increasing static pressure, and temporarily reversing flow. The system then recovers, resuming forward flow in cycles called pumping mode, which happens at short intervals. [2], [3].

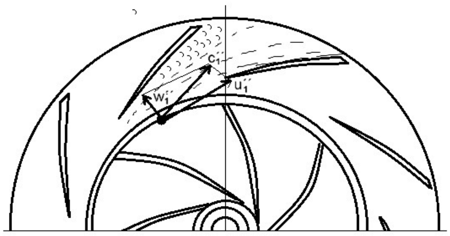

Figure 4 Flow separation on the suction side of the vane diffuser blades, $Q_v < Q_{v,cal}$.

2. VERIFICATION OF UNSTABLE OPERATION IN RADIAL COMPRESSORS THROUGH EXPERIMENTS

For a verification of the theoretical statement, we decided to make an experimental measurement with a decreasing inlet area in the turbine engine. Theoretically, when the engine runs at a steady rotational speed, this scenario is depicted as a movement along the n = const. line on the radial compressor characteristic, shifting to the limit of unstable operation [4], line on the compressor's performance curve, as shown in Figure 5. As the inlet airflow rate Q_v decreases, the operating point gradually nears and ultimately crosses into the previously established instability region, leading to what is known as the "pumping" phenomenon, as seen in Figure 6.

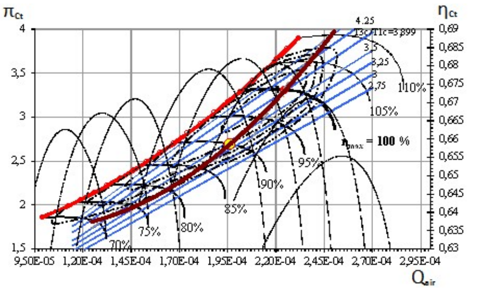

Figure 5 Characteristic of the radial compressor of the experimental small jet engine

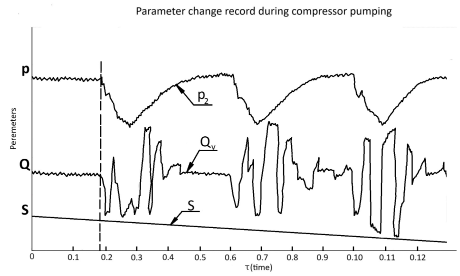

Figure 6 Logs of parameter variations during compressor surge

Experiments were conducted at the Technical University in Košice's engine lab using the MPM-20 turbojet, as seen in Figures 7 and 8. This small engine, with a diagonal inlet, single-stage centrifugal compressor, pooled combustion chamber, uncooled gas turbine, and fixed outlet nozzle, effectively examines airflow, compressor instability, and engine performance settings [4].

2.1. Throttling of the air flow in the intake system

To strengthen the theoretical basis, the experiments were accompanied by a comprehensive linear mathematical model of the MPM-20, developed using the small perturbations theory [1],[8],[10]. This model is tailored for subcritical flow conditions at the outlet nozzle and predicts that inlet variations significantly influence all critical operational parameters of the small turbojet engine.

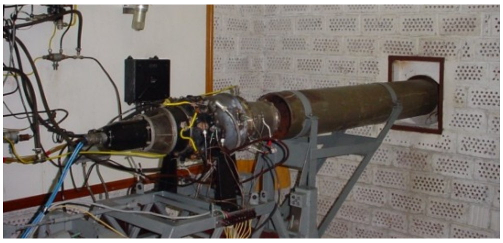

Figure 7 MPM-20 in the laboratory

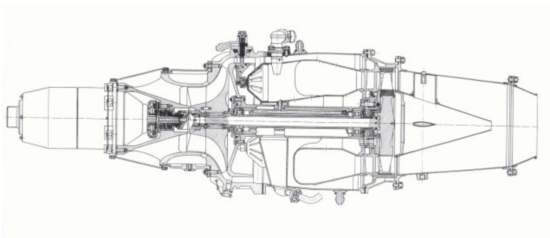

Figure 8 Cross-section of the small jet engine

We used four inlet setups with decreasing airflow surface to validate the model's predictions by throttling MPM-20. In each, we measured crucial engine parameters, comparing them against calibration benchmarks and theoretical values from small-change theory. The experimental setups were as follows:

1. The MPM-20 inlet with standard protective screen with a 2.5 × 2.5 mm mesh.
2. Inlet equipped with a mesh screen of 1.5 × 1.5 mm.
3. Dual-layer screen, combining 1.5 × 1.5 mm and 2.5 × 2.5 mm mesh.
4. Inlet covered with a perforated TV screen featuring 0.4 mm mesh

The change in the independent variable, the imposed disturbance, was quantified using Equations 2.1.1 and 2.1.2. These equations allowed for a precise measurement of how varying levels of inlet restriction affected the engine's performance.

$$\delta X_{si} = \left[\frac{X_{si} - X_0}{X_n}\right].100[\%] \qquad (2.1.1)$$

Where: δX_{si} - Change in the independent variable quantity, X_{si} - Value of the parameter at the simulated disturbance, X_0 - Original value of the independent variable quantity.

The change in the dependent variable variable was calculated according to the relation:

$$\delta Y_{si} = \left[\frac{Y_{si} - Y_0}{Y_n}\right].100[\%] \qquad (2.1.2)$$

Where: δY_{si} - Change in the dependent variable, Y_{si} - Value of the parameter under simulated disturbance, Y_0 - Original value of the dependent variable.

The initial experiment was conducted without the original inlet protection screen from the MPM-20 inlet system. Subsequent measurements were performed in an ideal environment per the technical documentation [9]. After taking 10 calibration measurements to establish an average, this will serve as a reference for later variations.

Calibration results align well with thermodynamic calculations for engine thermal circulation, as shown in Table 1. Minor differences in thermodynamic parameters result from measurement errors due to sensor placement differences from theoretical models.

Table 1 Comparison of calculated and measured parameter values during the calibration measurement

Parameter	Units	Measured Value	Calculated Value
pH	[Pa]	99885.82	101325.20
TH	[K]	290.65	288.00
Operation Time	[seconds]	50.80	50.00
p2,K′	[Pa]	180787.90	181600.13
p2C,K′	[Pa]	392652.70	398549.20
p2C	[Pa]	351971.50	392321.50
p3	[Pa]	351326.20	392321.50
p4	[Pa]	154655.78	162812.95
T2C′	[K]	458.55	462.35
T2C	[K]	460.25	462.35
T3C	[K]	1170.35	1168.15
T4C	[K]	1043.45	1013.27
Qpal	[cm^3/Cycle]	1362.00	—
Gpal	[kg/Cycle]	1.06	—
Ch	[$kg \cdot h^{-1}$]	74.87	—
FT (Thrust)	[N]	—	698.09
Gv	[$kg \cdot s^{-1}$]	—	1.20
cm (Specific cons.)	[$kg \cdot h^{-1} \cdot N^{-1}$]	—	0.13

2.2. Airflow with standard protective screen 2.5 × 2.5 mm

During the first measurement, ten measurements were taken using the original setup of the MPM-20 calibration run with the standard protective screen.

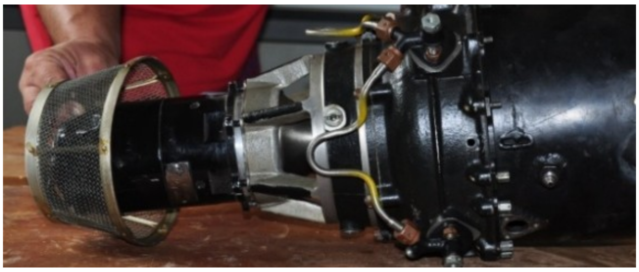

Figure 9 Removal of the protective screen from the MPM-20

This study assesses the effect of removing the inlet screen on engine performance. The initial inlet screen, constructed from 2.5 × 2.5 mm mesh wire with a thickness of 0.6 mm, can be seen in Figure 9, had a total area of 0.078593 m² and was subsequently removed.

Most parameters changed little, despite a 35% increase in inlet flow area. The static gas pressure after the turbine dropped 5.4%, and the total gas temperature rose 2.9%. Removing the inlet screen had minimal impact, confirming it was well-designed to protect while limiting performance loss. This test set a baseline for future studies.

2.3. Single fine mesh screen 1.5 × 1.5 mm

A mesh screen with a 1.5 × 1.5 mm grid and 0.3 mm wire, covering 0.078593 m² and 34.984% of the inlet, was installed to assess airflow and engine performance. Results closely matched the original screen's calibration, with no significant changes in thermodynamics or performance. Although it slightly restricts airflow, its effect on engine operation is minimal, making it compatible without performance issues.

2.4. Dual-layer mesh screen 1.5 × 1.5 mm + 2.5 × 2.5 mm

To test the impact of increased inlet resistance with dual mesh layers, a dual-layer screen was made by combining a 2.5 × 2.5 mm mesh with a 1.5 × 1.5 mm mesh, as shown in Figure 10, reducing the inlet flow area by 58%. Consequently, the turbine's expansion ratio rises by 19.194%, and downstream gas temperature increases by 4.475%. Other performance metrics also change accordingly. Elevated restrictions affect thermodynamic performance, including higher expansion ratios and temperatures, highlighting how increased inlet resistance impacts downstream performance conditions.

Figure 10 Dual screen of the MPM-20

2.5. TV screen 0.4 mm mesh

To assess the impact of extreme inlet restriction, a perforated sheet with 0.4 mm mesh, initially a TV screen shield, was placed over the engine's inlet. This change caused an 83% drop in effective inlet flow area.

Figure 11 TV screen on the MPM-20 intake system

Significant changes occurred in performance parameters during final tests. Pressure at station 2c dropped by 48,978.8 Pa, increased at station 3 by 24,198.5 Pa, and decreased at station 4 by 24,957.82 Pa.

Temperatures declined: station 2c by 11.6 K, station 3c by 92.4 K, and station 4c by 177.5 K. Fuel consumption decreased by 4.3465 kg/h. Pressure ratios changed: total compressor ratio ($\Delta\pi Tc$) increased by 0.6, $\Delta\pi Kc$ decreased by 0.509, and $\Delta\pi VD$ declined by 0.257.

Extended operation revealed engine instability: unstable radial compressor, damaged turbine blades, as seen in the Figure 12, and burned sealant, Figure 13 and 14. 83% inlet shading restricted airflow, reduced performance, and ultimately caused engine failure, showing that inlet restrictions beyond a threshold damage both performance and machinery.

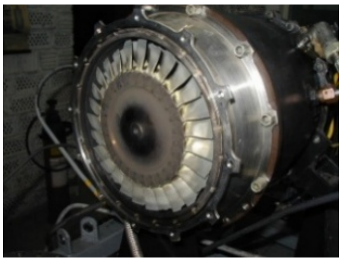

Figure 12 Damaged rotor blades of turbine

Figure 13 Burnt-out sealing compound in the gas turbine casing above the rotor blades

Figure 14 Engine on the fighter aircraft during final measurement

As a result of the final measurement, the turbine engine was burned out and unable to be used again. After all the results, we made Table 2, which collects all the following results of the measurements.

Table 2 The data coming from every measurement

Parameter	Unit	Without Screen	Basic Screen	Fine Mesh Screen	Dual-Layer Screen	TV Mesh (Ultra-Fine)
Inlet Area (Svst.)	[%]	100.00	80.00	65.00	58.00	17.00
pH	[Pa]	100525.30	100365.60	99885.82	100125.30	99991.98
TH	[K]	288.75	290.95	290.65	290.65	290.29
Time	[seconds]	51.00	49.70	51.70	49.70	50.00
p2,K′	[Pa]	178967.10	179136.70	180787.90	198319.40	213852.30
p2c,K′	[Pa]	388941.80	390028.10	391185.70	397633.70	428407.30
p2c	[Pa]	351178.40	390028.10	351971.50	366122.20	400157.20
p3	[Pa]	351524.70	351571.50	351326.20	340125.30	327326.20
p4	[Pa]	128716.48	128977.10	154655.78	154192.90	153674.30
T2c′	[K]	458.35	458.45	458.55	460.65	470.01
T2c	[K]	459.55	459.95	460.25	461.95	471.15
T3c	[K]	1169.25	1170.05	1170.35	1172.95	1261.65
T4c	[K]	1039.15	1041.15	1043.45	1085.65	1216.65
Qpal	[cm^3/cycle]	1407.00	1405.00	1397.00	1330.00	1293.30
Gpal	[kg/cycle]	109.05	10.89	752.90	10.31	10.03
ch	[kg/h]	770.07	788.70	752.90	747.43	726.60
FT	[N]	732.5*	731.6*	698.1*	598.74*	541.11*
cm	[$kg\cdot h^{-1}\cdot N^{-1}$]	0.1051283*	0.107811*	0.107847*	0.125334*	0.13428*

3. CONCLUSION

This study shows that instability in radial compressors can be caused by decreased inlet airflow. Using the MPM-20 jet engine, we confirmed predictions about instability regimes, including a shift to pumping when airflow drops below the design point. Four tests with decreasing inlet areas found that minor restrictions had little effect, moderate restrictions caused thermodynamic changes, and severe restrictions led to performance loss and increased fuel consumption, ultimately leading to mechanical damage to turbine damage. Excessive airflow restriction not only worsens performance but also risks severe instability and engine damage. Results closely match the model, validating its use for diagnosis. The findings emphasize the importance of airflow control, inlet design, and accurate modeling to maintain stability and safe operation. This research advances understanding of compressor limits and supports future efforts in surge reduction and engine management.

4. REFERENCES

[1] HOCKO, M., 2003. *Hodnotenie stavu LTKM na základe zmeny termodynamických parametrov*. Dizertačná práca. Košice: [Publisher if known], 338 pp.
[2] RŮŽEK, J., 1979. *Teorie leteckých motorů. Část I: Kompresory, turbíny a spalovací komory*. Brno: VA AZ, vysokoškolská učebnica, 373 pp.
[3] OTT, A., 1983. *Základy teorie a konstrukce leteckých lopatkových motorů. Část I*. Košice: VVLŠ, vysokoškolská učebnica, 140 pp.
[4] MED, S., [n.d.]. *Diagnostika JPM-TS-20 v laboratorních podmínkach K-316*. Diplomová práca. Katedra letadel.
[5] CUMPSTY, N. A., 1989. *Compressor aerodynamics*. Cambridge: Department of Engineering, University of Cambridge, 687 pp.
[6] HOCKO, M. and GAŠPÁR, R., 2013. Impact of rapid thermal fluctuations of the air flow into engine inlet to the gas-dynamics stability of the turbojet engine. *12th Conference on Power System Engineering, Thermodynamics & Fluid Flow*. Pilsen, 8 pp.
[7] HOCKO, M., 2003. *Malý prúdový motor MPM-20*. Košice: VLA.
[8] ČERKEZ, A. JA., 1975. *Inžinernyje rasčety gazoturbinnych dvigatelej metodom malych odklonenij*. Moskva: Mašinostroenie, 379 pp.
[9] *Provoz a technická obsluha motoru AL-7F-1. Kniha 2, Kniha 3*. 1965. Praha: Let-21-20/2, Let-21-20/3.
[10] FŐZŐ, L., ANDOGA, R. and MADARÁSZ, L., 2010. Mathematical model of a small Turbojet Engine MPM-20. In: *Studies in Computational Intelligence*, Vol. 313, pp. 313–322.
[11] HUNT, John W., 2021. *Radial Flow Turbocompressors: Design, Analysis, and Applications*. Cambridge: Cambridge University Press. pp. 565–600. DOI:10.1017/9781108241663.019P
Korba, Ozgur Balli, Hakan Caliskan, S. Al-Rabeei, U. Kale, Energy, exergy, economic, environmental, and sustainability assessments of the CFM56-3 series turbofan engine used in the aviation sector, Energy, Volume 269, 2023,126765, ISSN 0360-5442

Received 05, 2025, Accepted 06, 2025